Chapter 18
Clay Swelling: New Insights from Neutron-Based Techniques

Isabelle Bihannic, Alfred Delville, Bruno Demé, Marie Plazanet, Frédéric Villiéras, and Laurent J. Michot

Abstract Clayey materials are complex hierarchical and deformable porous media whose structure and organization vary at different spatial scales depending on external conditions, in particular water activity. It is therefore important, on the one hand, to follow all the structural changes that are associated with the adsorption of water molecules in the interlamellar spaces (at the scale of the particles) and, on the other hand, to describe the textural modifications induced at larger scales as a result of the swelling of individual particles. Neutron-based techniques are important to achieving this multiscale description, thanks to some special features of neutrons [e.g., specific interaction with hydrogen atoms, with in addition differential interaction with isotopes (H and D), and high penetration length of neutron beams, which allows easy preparation of versatile sample-cells container]. Finally, water dynamics in the interlayers can be investigated because of the unique interaction of neutrons with hydrogen.

After a brief discussion of the crystal chemistry of swelling clays, some examples of the application of neutron techniques to the study of clays will be given, including application of neutron diffraction to the study of the structure evolution of various expandable clays upon hydration and investigation of interlayer water dynamics by quasielastic neutron scattering (QENS) experiments, illustrating water molecule mobility as a function of hydration states. The difficulties in applying these techniques to materials with such complex crystal chemistry and anisotropic shape will be pointed out.

Clay hydration and swelling induce modification of aggregates at larger spatial scale than the nanometric one investigated by diffraction. Clay fabric and particles organization at the sub-micronic scale can be investigated by small-angle neutron scattering (SANS) experiments. Examples of SANS measurements will be given in the so-called crystalline swelling domain, for water activity below 1. In the clay–water system, as the solid/liquid ratio decreases, gels formation is observed in which individual clay layers are now separated by distances larger than a few

I. Bihannic (✉)
Laboratoire Environnement et Mineralurgie, UMR 7569 CNRS-INPL-ENSG, F-54501 Vandoeuvre Lès Nancy cedex, France
e-mail: isabelle.bihannic@ensg.inpl-nancy.fr

L. Liang et al. (eds.), *Neutron Applications in Earth, Energy and Environmental Sciences*, Neutron Scattering Applications and Techniques,
DOI 10.1007/978-0-387-09416-8_18,

nanometers. Experimental studies performed on clay suspensions or gels will be presented, demonstrating that clay layers are equilibrated in gels via electrostatic repulsions.

18.1 Introduction

Clay minerals are finely divided silicates that are ubiquitous in soils and sediments and are widely used in many industrial applications [1 and references within]. The following are among the numerous uses of one class of clay minerals, the bentonites:

- as plasticizing agents in ceramics;
- as binding agents in the pellitization of ores or other finely divided solids (application in foundries for moldings) or in the preparation of animal feed;
- as additives to improve the viscosity and rheological properties of drilling muds (petroleum industry);
- as soil additives in the construction of diaphragm walls or engineered barriers for waste management (civil engineering);
- as thickening agents for paints, varnishes, and cosmetics;
- as adsorbents in the food and beverage industries (e.g., for clarification of wines, beer stabilization, and, after acid activation, decolorizing vegetable and mineral oils); and
- as catalysts and catalyst supports in many organic syntheses.

Most of these uses are linked to the unique properties of clay minerals in terms of rheological behavior, water retention, and ionic exchange capacities—properties that are connected to their physicochemical characteristics.

One of the main features of clay minerals is their ability to accommodate important amounts of water in their structure, a phenomenon referred to as "clay swelling." The associated processes first occur at the nanometric scale within interlayer spaces and have strong consequences for various macroscopic behaviors such as mud rheology, swelling and shrinkage of soils, and slope stability. Furthermore, in applications where clay minerals are used as barrier materials, the transport of water and ions at large scale are somehow linked to the dynamics of water at the atomic level.

Scrutinizing changes in the structure of clays and in the dynamics of interlayer fluids as a function of water content obviously represents a mandatory prerequisite for unraveling swelling processes. It requires the use of techniques spanning several orders of magnitude in length and time to relate molecular properties to hierarchical structure, both evolving with water content. In that respect neutron scattering techniques are particularly relevant, as outlined by Dove in a special issue of the *European Journal of Mineralogy* on neutron scattering in mineral sciences [2]: "Neutron scattering methods have an astonishing versatility. . . . Since neutron scattering probes both the length and energy scales of atomic processes, it is possible to design experiments that focus on both spatial and dynamical processes at the same time, or else which focus on one or other." It can be added that the particular

sensitivity of neutrons to hydrogen atoms makes them powerful probes for analyzing water features (Chapter 2).

The importance of neutron techniques for studying clay minerals has long been recognized. Neutron diffraction [3–23], SANS [24–34], and quasielastic and inelastic scattering [23,35–50] have been applied to the study of different clay structures over the past 30 years.

In this chapter we will try to illustrate the versatility and specificity of neutron-based techniques for studying water–clay interactions on various scales. We will first focus on the use of diffraction and QENS to describe the structure and dynamics of interlayer water in different clay samples. We will then show how SANS can be used to analyze the evolution with increasing water content of the multiscale structure of compacted clay samples (i.e., in conditions that are compatible with the use of clay minerals in civil engineering and in barrier materials). Finally, we will show how SANS can be used to understand the structure of clay suspensions and clay gels.

18.2 Clay Structure and Organization

Clay minerals are phyllosilicates whose unit structure is a layer built from the stacking of sheets of tetrahedrally coordinated cations (tetrahedral layer T) and octahedral (O) sheets of oxygens and cations [51]. Tetrahedra are mainly occupied by silicon, while octahedra are mainly occupied by either aluminum or magnesium. Various clay minerals may be defined depending on the nature of the aforementioned assemblage. The entity of one tetrahedral sheet and one octahedral sheet yields the so-called 1:1 layer silicate structure or TO structure. It is the one encountered for kaolinite (Fig. 18.1). In the 2:1 layer silicate structure (also called TOT structure), two silicon tetrahedral layers sandwich an octahedral layer. This is the case for smectite (swelling clays) and for mica and illite (Fig. 18.1).

Cations other than silicon, aluminum, or magnesium can fit into the voids of the tetrahedral and octahedral polyhedra. When these isomorphic substitutions lead to charge unbalance, electroneutrality is ensured by the counter-ions (cations) located

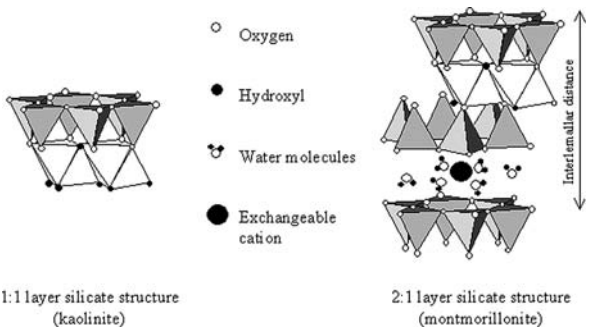

Fig. 18.1 Schematic representation of the layer structure of clay minerals

Table 18.1 General classification of 2:1 phyllosilicates

Charge/ unit cell	Dioctahedral clays	Trioctahedral clays
0	Pyrophyllite	Talc
	$(Si_8)(Al_4)O_{20}(OH)_4$	$(Si_8)(Mg_6)O_{20}(OH)_4$
0.4–1.2	**Montmorillonite**	**Hectorite**
	$(Si_8)(Al_{4-x}Mg_x)O_{20}(OH)_4CE^{z+}_{x/z}$	$(Si_8)(Mg_{6-x}Li_x)O_{20}(OH)_4CE^{z+}_{x/z}$
	Beidellite	**Saponite**
	$(Si_{8-x}Al_x)(Al_4)O_{20}(OH)_4CE^{z+}_{x/z}$	$(Si_{8-x}Al_x)(Mg_6)O_{20}(OH)_4CE^{z+}_{x/z}$
1.2–1.8	Illite	Vermiculite
	$(Si_{8-x}Al_x)(Al_{4-y}Mg_y)O_{20}(OH)_4K^+_{x+y}$	$(Si_{8-x}Al_x)(Mg_{6-y}Cat^{3+}_y)O_{20}(OH)_4CE^{z+}_{(x+y)/z}$

Note: Mineral names in bold correspond to smectites.

in the interlamellar spaces. Most properties of swelling clays (e.g., ion exchange properties or water retention) result from the presence of such mobile exchangeable and hydratable cations. A brief classification of clay minerals is given in Table 18.1, which defines the structure and formula of clays mentioned in this chapter. The generic name "smectite" corresponds to the swelling clays reported on row 2 of Table 18.1 (i.e., when the charge of the unit cell is not too high to prevent swelling). Even though vermiculite presents swelling properties under some conditions, this mineral does not belong to the "smectite group," as swelling is limited due to the higher charge of vermiculite compared to that of the smectites.

The basic unit of clays comprises the TO layer (or TOT layer) and associated interlayer space. These units are platelet-shaped and can be considered two-dimensional (2D), with a thickness around 1 nm and a lateral extension that is extremely variable (from a few nanometers to a few microns). The stacking of these units then forms particles.

Cohesion between layers inside particles is strongly dependent on parameters such as charge density and location (tetrahedral or octahedral sheet) and the nature and valence of the exchangeable cations. Cohesion affects crystallite morphology. For example, in micas or illite, where attraction between layers is strong and counter-ions are abundant, the resulting stacking is regular. Also, adjacent 2:1 layers are keyed into positions that prevent mobility and exchange of interlayer counterions. Conversely, smectites, which have a lower charge compared to micas, are characterized by extremely disordered and irregular stacking. In such cases, there are no rules for defining the relative positions and orientations of adjacent layers, and the stacking thus formed is referred to as turbostratic. Considering the high polydispersity of the in-plane dimension of the layers, the notion of particle becomes difficult to picture, the layer stacking leading to a more or less continuous and disordered assembly.

The assembly of layers and particles in such a hierarchical structure generates voids, beginning with the interlamellar spaces. Within particles, stacking defaults such as irregularities in the distances sequence also give rise to lenticular pores, with thickness down to a few nanometers. At larger scales, voids existing between

particles or aggregates of particles correspond to mesopores or macropores.[1] The morphology of the porous network is strongly related to the solid phase geometry and is also hierarchically organized [53].

This general picture of the clay fabric is strongly modified in the presence of water, as swelling (or water uptake) corresponds to an expansion of interlayer spaces due to penetration of water molecules into the interlamellar regions. Since the pioneering work of Norrish [54] on sodium–montmorillonite, clay scientists commonly distinguish two swelling stages: intracrystalline and osmotic swelling. Intracrystalline or crystalline swelling occurs for the lowest water contents (under-saturated systems) and corresponds to the first hydration steps of interlamellar spaces, mainly through interlayer cation hydration [55–66]. This process occurs in a stepwise manner as a function of water activity. The apparent interlamellar distance (d001) increases step by step from a value around 9.5 Å for the dry state to roughly 12.5 Å for a state referred to as water monolayer state (the increment of 3 Å corresponds to the size of the water molecule). As water activity increases, the interlamellar distance reaches 15.5 Å for the so-called bilayer state. The domains of existence of the different states, as well as the exact d001 value, strongly depend on the cation nature and on the amount and localization of charges in the TOT layer [62, 63]. On the basis of experimental work [water adsorption measurements and X-ray diffraction (XRD) studies] performed on montmorillonite and hectorite, it appears that cation hydration is the main parameter which governs water uptake and swelling. In most cases, interstratified phases of zero hydrates or one-, two-, and sometimes three-layer hydrates are encountered [61–63]. On the contrary, tetrahedral charge localization leads to more homogeneous hydration states, with marked swelling steps as seen by X-ray diffraction [58, 59], thereby revealing the importance of charge localization on water structure, in line with simulation results [67]. Close to saturation (water activities around 0.98), another regime begins and is referred to as osmotic swelling. For monovalent cations, it corresponds to a continuous expansion of clay layer spacing with increasing water content. [54, 56, 64, 65].

From a structural and textural point of view, the penetration of water molecules into the interlamellar spaces locally generates significant volume variations. For instance, the volume increase of a particle upon hydration from the dry state to the one-layer hydrate state is about 30% (ratio 9.5:12.5 Å). The expansion of the interlayer spaces occurs at the expense of the porous network as macroscopic swelling is only visible for the highest water activities. Furthermore, as hydration goes on, capillary condensation will lead to the filling of the smallest pores. The hydrated clay material is then a complex system with domains where water exists under different status: confined water in the 2D interlayer spaces and bulk water filling mesopores. Macroscopically, this will affect the transport properties of water molecules and ions.

[1] According to the IUAPC convention [52], pores are characterized by their diameters, where micropores (<2 nm), mesopores (26–50 nm), and macropores (>50 nm) are identified.

18.3 Crystalline Swelling: Structure and Dynamics of Water Molecules in the Interlayer Spaces

18.3.1 Structural Description of Crystalline Swelling

On the basis of the clay description provided in the previous section, swelling clearly appears as a phenomenon that is initiated at the molecular level by the solvation of interlayer cations. This is accompanied by structural changes of these semicrystalline materials (water uptake involves a few angstroms increase of the interlamellar distances). Therefore, neutron or XRD techniques where the wavelength of incident beams is of the same order as the interatomic distances are particularly relevant to following the structural changes occurring upon hydration. The applicability of XRD to studying crystalline swelling of hydrated smectites has been recognized for more than 70 years, as shown by the number of publications based on this technique (the list given here being inevitably partial) [54–65,68, 69]. The frequent occurrence of the use of XRD is linked to the ubiquitous availability of the technique in laboratories, even though there are strong limitations to its use for probing the structural details associated with light elements such as hydrogen. In contrast, neutron scattering lengths are not dependent on electronic densities, and the contribution on scattering of light elements, which have scattering lengths on the same order as heavy elements, is significant (Chapter 2). In addition, neutron scattering lengths are isotope-dependent. For instance, neutron scattering lengths for H, D, Si, and Al are −3.74, 6.67, 4.15, and 3.45 fm, respectively. Thus, structural studies of water in hydrated crystals are possible and largely benefit from the isotopic dependence on scattering length. Using H_2O/D_2O exchange yields additional information that is helpful in getting the precise location of hydrated species.

The large variability in textural properties and crystal chemistry of swelling clays was emphasized in the first paragraph of Section 18.2. Depending on the clays studied, the approaches to interpreting results from neutron diffraction to get the structural configuration of water molecules in the interlayer spaces will differ. In the following subsections, we will give some examples of the work performed on different expandable clays (vermiculite, montmorillonite, and saponite).

18.3.1.1 Vermiculite

Vermiculites are 2:1 clay minerals, with a charge deficit that mainly arises from the tetrahedral layer. The relatively high charge prevents a continuous expansion of the interlayer at high water contents. At low water contents, vermiculites present well-defined hydration steps [70] along the water adsorption isotherms. Experimentally, it is then easier to control the hydration states that are studied. Furthermore, vermiculites sometimes occur as macroscopic crystals [7], making perfect orientation of samples possible.

Skipper and coworkers undertook a complete description of the interlayer structure of vermiculite, with either monovalent counter-ions (Li^+ [9], Na^+ [7]), or

divalent counter-ions (Ca^{2+} [8], Ni^{2+} [7]). The method used to derive the interlayer distribution of cations and water molecules is based on an inverse Monte Carlo simulation in which the neutron scattering density profile along the z-axis perpendicular to clay layers [ρ(z)] is calculated from the integrated intensities of the (00l) reflections.

Intensities are related to $\rho(z)$ by the following formulae:

$$I(q) = M(q)|F(q)|^2, \tag{18.1}$$

and

$$F(q) = \int_{-c/2}^{c/2} \rho(z) e^{iqz} \mathrm{d}z. \tag{18.2}$$

Intensity is expressed as a function of the modulus of the scattering vector q [$q = 4\pi \sin(\theta)/\lambda$, where 2θ is the scattering angle and λ the wavelength], c is the layer spacing, $M(q)$ is a function that takes into account textural effects (size of sample and orientation), and $F(q)$ is the structure factor. Diffraction patterns were recorded after equilibrating the samples with either H_2O or D_2O. This leads to two different density profiles, one for hydrogen atoms and the second one for the clay layer plus oxygen atoms. An example of neutron scattering density profiles obtained in this way on lithium–vermiculite is given in Chapter 17 of this volume.

The experiments carried out on Li-, Ca-, and Ni-vermiculites [7–9] reveal that in the water bilayer state, these cations are solvated by six water molecules forming octahedral hydration complexes, giving rise to more ordered interlayers than for sodium–vermiculite [7].

The swelling behavior of vermiculites is strongly modified when exchangeable cations are replaced by organic counter-ions such as propylammonium [13], with which a further expansion of interlayers is observed. For such compounds, the H/D isotope labeling can also be exploited to describe in detail the colloidal behavior of such phases. The same approach was applied using other organic compounds such as polyethylene oxide or butylammonium ions [17].

Finally, the versatility of neutrons for studying samples in conditions mimicking deep environments is illustrated in the experiments of Skipper et al. [15], where the swelling of vermiculites was followed under fluid pressures of up to 1.5 kbar and temperatures of up to 300°C. The authors took advantage of the low absorption of neutrons by some alloys with high mechanical resistance to conduct experiments in temperature and pressure conditions analogous to those encountered in sedimentary and basin conditions.

18.3.1.2 Montmorillonite

Vermiculites present typical hydration properties, but are not representative of the most common swelling clays encountered in the environment or in industrial applications. The most frequently encountered smectites are montmorillonites and

beidellites. Their swelling behavior cannot be directly derived from that of vermiculite due to their smaller crystallite size (less than a micrometer) and different charge amount and location, which lead to much less well-defined hydration steps. Cebula et al. [3] undertook a complete experimental diffraction study on a series of monovalent exchanged montmorillonites by combining (1) experiments in classical diffraction conditions to follow the evolution of the (00l) reflections as a function of relative humidity, (2) mosaicity evaluation by measuring the intensity of (001) Bragg peaks for different positions of samples relative to the neutron beam to get a degree of platelets ordering, and (3) small-angle scattering measurements. The main conclusion of this work is that there are no significant structural differences depending on the nature of the exchangeable cation and that all samples are characterized by a strong disorder in the arrangement of clay platelets and a spread distribution of spacings along the *c*-axis. A more detailed description of the water molecules in the interlayers could not be achieved as the intensities of the (00l) harmonics were very weak. This comes from the use of H_2O to hydrate samples, as will be discussed in the next section on saponite. When D_2O is used instead of H_2O, (00l) reflections present more intense diffraction peaks [4], enabling a one-dimensional (1D) Fourier transform of intensity to get scattering density profiles. This approach conducted on a sodium-montmorillonite revealed that the interlayer water was not highly structured. For some hydration rates the interstratification between different hydrated states leads to continuous diffraction curves, hindering high resolution in the treatment.

Swelling depends on the nature and valence of counter-ions present in interlamellar spaces. With neutron scattering, the differential neutron interactions with isotopes can be taken advantage of to study the cation environment in interlayer spaces. Thus, Powell et al. and Pitteloud et al. [11, 12, 16] used both H/D and ^{6}Li/^{nat}Li or ^{58}Ni/^{nat}Ni isotopic substitutions to describe the two-layer hydrates in lithium- and nickel-montmorillonite. In their approach, pair radial distribution functions describing the interlayer molecules are evaluated via Fourier transform of difference functions calculated by subtracting the intensities recorded in the same conditions with two isotopes. This method is explained relative to pollutant speciation in water in Chapter 17 of this volume. For nickel, it was established that the hydration shell of this cation is made up of six water molecules arranged octahedrally but with some distortions. Additional water molecules adopt a liquid-like structure, which is also observed with lithium. The structure of the coordination shell around lithium was not derived.

A detailed knowledge of the hydration behavior of montmorillonite is crucial to understanding swelling, which plays a crucial role when this expandable mineral is used as a barrier material. In the particular context of hazardous wastes disposal, where compacted clay barriers are used to inhibit pollutants and contaminants migration [71], a precise description of smectite hydration behavior is critical to assessing the engineered barrier sealing properties that may evolve depending on external conditions (humidity and temperature gradients for instance). Besides, additional constraints arise from the fact that, in barriers, clayey materials are compacted and confined. The issue to be addressed is whether crystalline swelling in

such materials still occurs even when macroscopic swelling cannot take place. In that case, neutron diffraction techniques are particularly relevant, as neutron beams can penetrate through the walls of sample holders (Chapter 2).

Neutron diffraction experiments were carried out on samples compacted at different apparent densities and undergoing swelling in isochoric conditions [22]. To reach these conditions, compacted clay pellets were placed in the special cells designed to stand the high swelling pressure developed for the most hydrated samples and allowing hydration by water molecules in vapor phase, thanks to a porous ring. Samples were equilibrated during many weeks in atmospheres where the relative humidity was controlled using various saturated salt solutions.

The experiments revealed that confinement does not prevent crystalline swelling, the evolution of the (001) reflections being similar on such samples and on samples free to swell. The influence of confinement is only observable for the most hydrated bentonite pellets ($P/P_0 = 0.98$), where peaks are bimodal, corresponding to an interstratified state with two and three water layers. Additional mosaicity measurements were also performed on the two kinds of samples studied [a montmorillonite and a bentonite (montmorillonite plus accessory minerals)]. As compared to montmorillonite, the texture of bentonite is only slightly affected by compaction, owing to the accessory phases that limit the orientation of clay aggregates during compaction.

18.3.1.3 Saponite

Studies on natural montmorillonite revealed, on some domains of relative pressure, the existence of interstratified hydration states [4,61–63] whose origin may be assigned to the heterogeneity of these minerals. Tetrahedral charge localization in natural clays such as beidellite or saponite leads to more homogeneous hydration states, with marked swelling steps as seen by X-ray diffraction [58, 59], thereby revealing the importance of charge localization on the water structure, in line with simulation results [67]. In contrast to montmorillonite, saponite is easily synthesized [21, 50, 60]. Synthetic saponite then represents a valid model system for natural clays. The use of synthetic samples with well-identified structural formulas is also a clear advantage when molecular simulations are implemented.

The hydration and swelling of this synthetic saponite has been the object of a multidisciplinary experimental and numerical study [21]. Water adsorption results are presented in Fig. 18.2, together with the evolution of the d001 interlamellar distances recorded by XRD for three saponites with different charges. By carefully looking at the monolayer state that corresponds to the first plateau on Fig. 18.2B, one can see that in the first part of this plateau, for relative pressure below 0.3, the three samples exhibit similar interlamellar distances, whereas for the most charged sample, the adsorbed amount of water can be twice the quantity adsorbed for the lowest charge. For a particular relative humidity, when looking at structure, the three samples appear to be in a similar state, but that is not the case for the quantity of water adsorbed. This emphasizes the necessity of finely characterizing each sample by comparing the data obtained from independent techniques yielding either

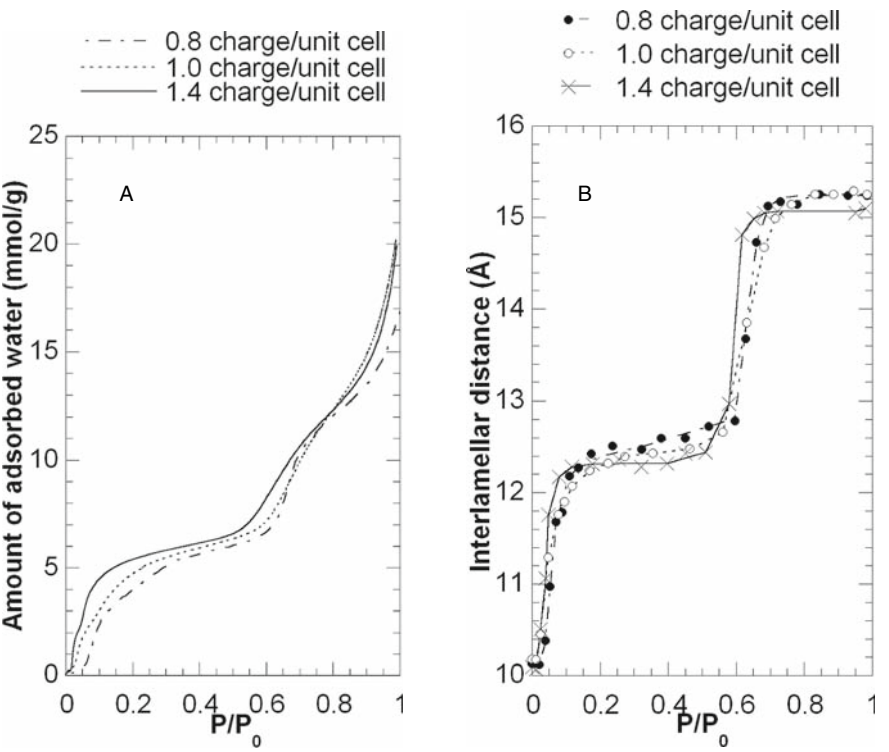

Fig. 18.2 **A**. Water vapor adsorption–desorption isotherms obtained on saponites with different charges. **B**. Associated evolution of the apparent d_{001} measured by X-ray diffraction (adapted from [60])

structural information or quantitative data with that for different domains of the water adsorption–desorption isotherm. For one of the samples (sodium-exchanged saponite with 1.0 charge per unit cell), neutron diffraction experiments were performed on the "small momentum transfer diffractometer D16" at Institut Laue-Langevin (ILL) [21]. The diagrams presented in Fig. 18.3 were recorded as a function of the partial water vapor pressure with either H_2O or D_2O. While for H_2O, the (001) reflection is very intense and shifts from 15.2 Å for the most hydrated state to 10 Å for the dry one, with an associated decrease in intensity due to the evolution of the structure factor, the D_2O (001) reflection vanishes (Fig. 18.3B) for a particular relative humidity ($P/P_0 = 0.38$).

By comparing the results obtained by near-infrared and Raman spectroscopy with structural results and the quantitative data obtained by water gravimetry, the following picture of this particular hydration state is obtained: interlayer cations are hydrated and interlamellar spaces are opened at 12.5 Å. Spectral results and simulations indicate the development in the interlayer of a disordered percolating hydrogen bond network [21]. To go further in the understanding of this particular

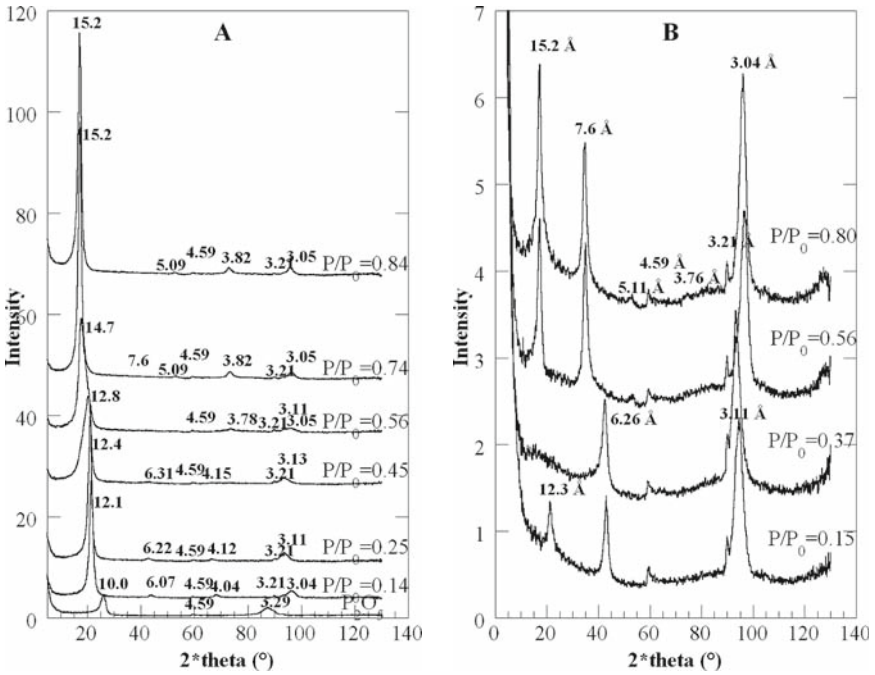

Fig. 18.3 Neutron diffraction patterns obtained in desorption for saponite. **A**. H_2O and **B**. D_2O (from [21], reprinted with permission from J. Phys. Chem. B **109**, 23745–2759 (2005). Copyright 2008 American Chemical Society)

feature, it is worth coming back to the formalism describing diffraction by lamellar structures [61, 72].

If we consider diffraction by stacks made of M identical layers distant from d_{001}, the expression of intensity for the (00l) reflections and in a direction perpendicular to the stack is as follows (z corresponds to the projection of the scattering vector q along the c-axis):

$$I00(z) \propto |F00(z)|^2 \sum_M \frac{\alpha(M)}{M} G00(z), \tag{18.3}$$

where $\alpha(M)$ is the distribution of stack thickness.

Intensity is then a product of two terms:

$$F_{00}(z) = \sum_{j=1}^{n} a_j f_j \exp(izzj). \tag{18.4}$$

$F_{00}(z)$ is the structure factor and represents the diffraction by all atoms and ions that constitute the layer plus atoms and ions of the interlayer. Each atom is

characterized by its scattering length f_j and its abundance a_j at the position z_j. The structure factor corresponds to the Fourier transform of the atomic distribution of the layer:

$$G00(z) = \frac{\sin^2(M\pi z d_{001})}{\sin^2(\pi z d_{001})}. \tag{18.5}$$

$G_{00}(z)$ is the modulation function as derived by Méring in 1949 [73]. This function expresses the distribution of intensity at angles that correspond to the Bragg law. This periodic function presents peaks for z values inversely proportional to d_{001}. The peak width is inversely proportional to M, which corresponds to the size of the diffracting domain.

In the overall expression of intensity, $F_{00}(z)$ contains all the information relative to the nature of scattering elements (position, number, etc.), and $G_{00}(z)$ corresponds to the structural information (distances between planes, size of particles).

The above expression does not take into account the whole complexity of turbostratic systems, where there is no ordering between adjacent layers. More complete calculations that are not presented here can be performed for adjusting calculated and experimental patterns [61]. Still, Eq. (18.3) can be used to illustrate the influence of water content on the shape of the diffraction patterns. Results are displayed in Fig. 18.4 for both D_2O and H_2O for either 2.5 or 3.5 molecules per cation. Figure 18.4 clearly shows that the squared structure factor is very sensitive to the amount of D_2O molecules present in the interlayer. Such a sensitivity is not observed with H_2O, for which $F^2{}_{00}(z)$ first decreases strongly for the smallest values of z and then presents small oscillations, but without any strong dependence on the number of water molecules. The other striking feature of the evolution of $F^2{}_{00}(z)$ when calculated with D_2O is the presence of minima for a z value of 0.5. The minimum is partial with 3.5 water molecules and tends to zero with 2.5 water molecules. This value of z also corresponds to a maximum of the interference function when $G_{00}(z)$ is calculated with d_{001} equal to 12.55 Å (note that this function is the same for both H and D, as it is only linked to structural parameters). The resulting intensity then displays a disappearance of the 001 reflection for a particular amount of water around cations. This illustrates the high sensitivity of the shape of diffraction patterns toward the number of water molecules when samples are equilibrated with D_2O. It should also be possible to refine the amounts and positions of water molecules by calculating the diffraction patterns from the atomic positions derived from grand-canonical Monte Carlo (GCMC) simulations.

18.3.1.4 Conclusion on Diffraction

As shown in the previous sections, neutron diffraction can provide fruitful information about the atomic distributions of atoms and molecules (especially water molecules) in the interlayer spaces of clay minerals. Such information can be obtained either from a direct interpretation of the diffraction patterns or through an indirect approach using independently measured parameters (GCMC, adsorbed

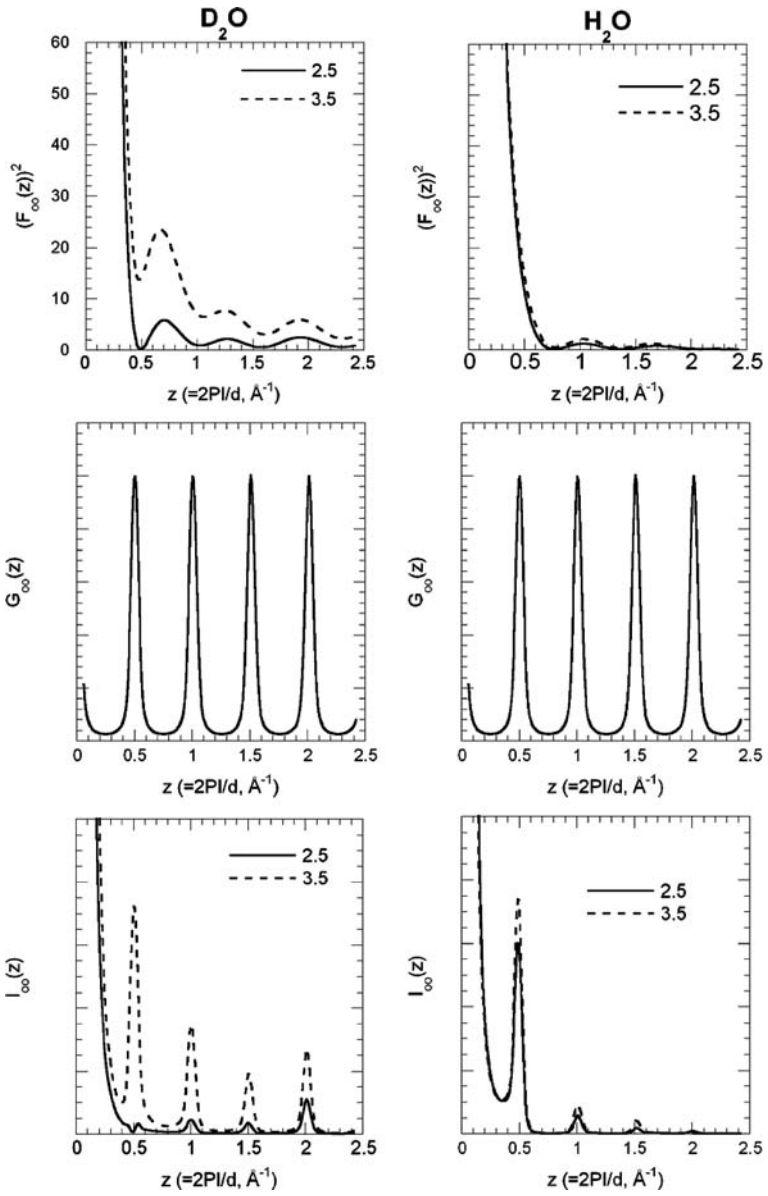

Fig. 18.4 $F^2_{00}(z)$, $G_{00}(z)$, and $I_{00}(z)$ calculated as a function of the water content (2.5 or 3.5 water molecules per cation), either with D_2O or H_2O

amounts, etc.). In any case, in carrying out either approach it is crucial to couple diffraction experiments with a precise characterization of water adsorption features and to achieve a very accurate control of humidity conditions when performing diffraction experiments.

18.3.2 Dynamics of Water—Quasielastic Neutron Scattering

As shown in the previous section, using neutron diffraction techniques in combination with other experimental methods, it is possible to obtain detailed snapshots of water and cation organization upon increase of water chemical potential. In many applications dealing with clay minerals, such a description remains incomplete because the dynamical properties of interlayer species cannot be obtained using such techniques. On the nanometric scale, and for time windows shorter than 100 ns, QENS techniques [74–76] are suitable for studying proton dynamics and therefore water mobility. The associated spatial and temporal scales also match those investigated by molecular dynamics, making cross-checking possible.

Diffusive motions like atomic translations and molecular rotations give rise to quasielastic signals, which originate from neutrons experiencing small energy transfers. Quasielastic intensity appears as a broadening of an elastic peak. Because hydrogen has a much larger incoherent cross section than any other atom, the signal of hydrogenated compounds is dominated by the self-particle dynamics of hydrogen. In QENS studies of hydrated clay minerals, the obtained spectra are therefore dominated by the motion of water molecules. Various quasielastic neutron scattering techniques are available for studying water dynamics: time of flight (TOF), backscattering (BS), and neutron spin echo (NSE) (Chapters 2 and 3). In the case of clay minerals, most studies have been performed using the TOF technique [35–42,45–50], while fewer studies have taken advantage of NSE [23, 43, 44, 46, 48] or BS spectrometers.

In a TOF spectrometer, neutron energy is deduced from the time it takes neutrons to travel a known distance (their TOF), whereas the scattered intensity is measured as a function of scattering angle (momentum transfer) and TOF (energy transfer). The instrumental resolution and accessible q-range essentially depend on the wavelength of the incident beam, which can be continuously adjusted on a TOF machine. The signals result from a convolution of a resolution (instrumental) function by the scattering function or dynamical structure factor denoted as $S_{\mathrm{inc}}(q, \omega)$, where q is the modulus of the scattering vector and ω the energy transfer (inc refers to incoherent scattering, which is dominant for hydrogen). Characteristic rotation and translation times can then be inferred from the modeling of the evolution of the broadening and intensity of $S_{\mathrm{inc}}(q, \omega)$ as a function of q.

To illustrate how QENS can be used for obtaining dynamical information on water motions, typical QENS spectra obtained for a synthetic saponite sample with a layer charge of 1.4 equilibrated at a relative water pressure of 0.84 for two values of the incident wavelength are given in Fig. 18.5. These spectra show the resolution function whose width depends on wavelength, various quasielastic signals modeled by Lorentzian functions, and an elastic peak present in the resolution function. This latter peak is due to the clay layer, especially the structural hydroxyl groups as well as to the water molecules whose motions are slower than the time window corresponding to the resolution function.

The quantity of probed mobile atoms can be derived from the calculation of the elastic incoherent structure factor (EISF), which is the ratio between elastic and total

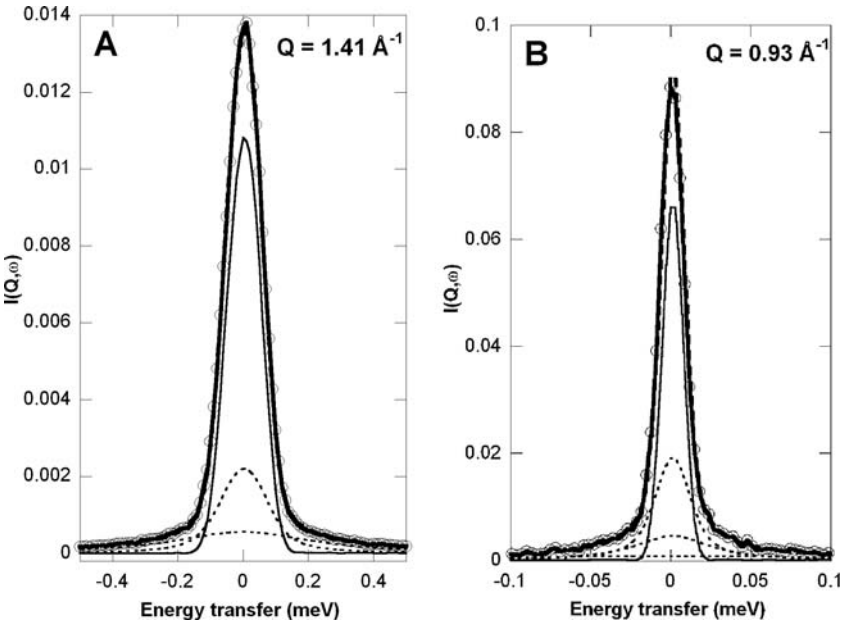

Fig. 18.5 Quasielastic spectra obtained by the time-of-flight technique for a synthetic saponite with layer charge of 1.4 per unit cell equilibrated at a relative water pressure of 0.84. **A**. $\lambda = 5$Å. **B**. $\lambda = 10$Å (adapted from [50])

scattered intensities:

$$\text{EISF} = \frac{I_{\text{elast}}(q)}{I_{\text{elast}}(q) + I_{\text{inelast}}(q)}. \tag{18.6}$$

In the case of clay minerals, knowing the amount of water adsorbed for each point, it is easy to calculate the EISF corresponding to the structural protons of the layer. The comparison between this value and the experimental EISF then provides the proportion of adsorbed water molecules probed in the experiment. The evolution of the EISF with q also provides information about confinement geometry, which is particularly relevant for clay minerals that, as already mentioned repeatedly in this contribution, are strongly anisotropic.

Analyzing the q dependence of the width of the quasielastic Lorentzian functions, it is possible to obtain the nature and characteristic times of the various motions of interlayer water molecules and to follow the evolution of these motions with water pressure. In clay minerals, two rotational components and one translational component have generally been observed ([41] and references within, [42]). As far as rotations are concerned, the faster rotational motion (characteristic time around 2 ps) appears roughly independent of the adsorbed water amount and is assigned to water molecules bound to interlayer cations while the slower one (around 20–40 ps) is related to the planar rotation of water molecules in hydration spheres around the

cation. This latter motion depends on both the hydration state and the nature of the interlayer cation.

Concerning translational diffusion, motions are significantly faster in the bilayer region as compared to the monolayer domain and are lower than that obtained for bulk water (2.3×10^{-9} m^2/s) [41]. As an example of typical values, Fig. 18.6 shows the radial translational diffusion coefficients obtained on a saponite sample together with those measured independently by molecular dynamics simulations. The values of translational diffusion coefficients reported in the literature [40–46,48–50] depend on the nature of the clay minerals and on the interlayer cation. They are also dependent on orientation, in-plane motions being faster than those perpendicular to the plane.

As noted previously, the time window accessible to TOF experiments remains limited in the high time region due to the relatively high width of the resolution function. For that reason, TOF experiments could certainly be complemented by BS experiments, which allow reaching higher resolutions (typically 1 μeV).

Another option to enlarge the time window is provided by the NSE technique, which preferentially enables the measurement of coherent signal and is the only neutron technique that gives a measurement of the intermediate function, $S(q,t)$, and covers relaxation times up to hundreds of nanoseconds (Chapter 3). Recent

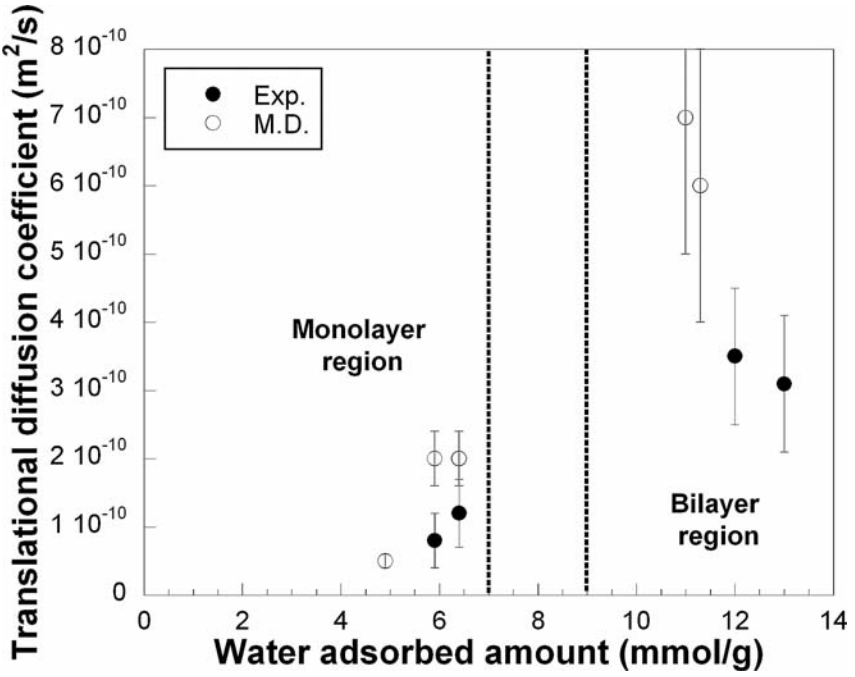

Fig. 18.6 Evolution of the experimental and simulated translational diffusion coefficients as a function of the amount of water adsorbed for a synthetic saponite clay with a layer charge of 1.4 per unit cell (adapted from [50])

publications coupling experiments and simulations [23, 46, 48] have indeed nicely shown the potential of this technique for studying water dynamics in confined interlayer spaces. However, up to very recently the diffusion coefficients obtained by TOF, NSE, and BS exhibited significant differences [42, 43, 46, 48]. In addition, the intermediate scattering functions $I(q,t)$ obtained from NSE experiments are generally better fitted using stretched exponential functions than monoexponential functions, especially to reproduce the experimental data at high q values. This behavior and discrepancy may be attributed to several phenomena.

1. At high q values, beyond 0.8 $Å^{-1}$, rotational contributions increase and lead to a decrease in the stretch exponent used to simulate the experimental data.
2. In the case of natural clay systems, structural heterogeneity in terms of chemical composition and layer charge leads to a distribution of water motions.
3. As shown very recently [23], imposing an isotropic analysis to a powder-averaged 2D diffusion model by using a stretched exponential fit results in an underestimation of diffusion coefficients by approximately 25%. By taking anisotropy into account, in the case of a synthetic fluorohectorite system, it was then possible to reconcile TOF and NSE measurements to yield similar diffusion coefficients.
4. Even taking into account all these possible reasons, microscopic simulations still reveal a non-monoexponential behavior for $I(q,t)$ [23]. This tends to reveal that a range of relaxation times is certainly present in the system and that describing the motion of interlayer water molecules with a single relaxation time may not be correct.

Despite all these limitations, and the complexity of data treatment, neutron scattering techniques still represent a unique tool for investigating interlayer water dynamics in clay minerals and their evolution with water content.

18.4 Clay Large-Scale Structure

Clayey materials are complex hierarchical and deformable systems whose structure and organization vary at different length scales depending on hydration conditions. The mesoscopic scale (i.e., a few angstroms to 1 μm) can be probed by small-angle scattering measurements (Chapter 2). In the present section, we will first recall some basic expressions of SANS and then show the application of this technique to two cases: (1) porosity changes induced by increasing water activity in confined clay materials and (2) the structure of clay suspensions and clay gels.

18.4.1 Principle of Small-Angle Scattering

Scattering phenomena result from the existence of heterogeneous domains with different scattering length densities at a submicronic length scale (for X-rays and

neutrons). The incident beam is scattered at the interface between these regions with different contrast. These domains can be either particles in a solvent or pores distributed in a matrix, and the features of the scattering pattern are related to the quantity, shape, and size of the scatterers. The purpose of small-angle scattering experiments is to deduce the scatterers' characteristics from the pattern.

A comprehensive description of small-angle scattering can be found in reference text books on this subject [77–79], and only very basic expressions will be recalled here.

The expression of intensity in a system with no interaction between scatterers is

$$I(q) \propto \overline{\Delta\rho^2} F(q). \tag{18.7}$$

$\overline{\Delta\rho^2}$ describes the fluctuations of scattering length density, and in the case of a biphasic system where phases 1 and 2 are characterized by their respective scattering length density ρ_1 and ρ_2 and their respective volume fraction ϕ_1 and ϕ_2, this term can be written

$$\overline{\Delta\rho^2} = (\Delta\rho)^2 \phi_1 (1 - \phi_1). \tag{18.8}$$

For diluted systems, ϕ_1 is negligible as compared to 1 and $\overline{\Delta\rho^2} = (\Delta\rho)^2 \phi_1$. The form factor is $F(q)$, and it contains the geometrical information about the scattering phase; for instance, for bidimensional objects $F(q)$ varies as q^{-2}, whereas for linear objects, $F(q)$ scales as q^{-1}.

For interacting particles, an additional term is contained in the expression of intensity:

$$I(q) \propto \overline{\Delta\rho^2} F(q) S(q). \tag{18.9}$$

The interference function $S(q)$ describes the interaction between objects.

18.4.2 Clay Texture in the Crystalline Swelling Domain

As mentioned in Section 18.3.1.2, compacted clays are used as barrier materials in hazardous waste containment. In the context of nuclear waste disposal, compacted clay materials are placed around canisters containing radioactive wastes [80, 81]. Changes in temperature and humidity occur, leading to textural changes. Such changes can be followed by SANS on compacted clay pellets. In that case, SANS presents a definite advantage over X-ray techniques as samples can be investigated under isochoric conditions [22]. Indeed, due to the high penetrating power of neutrons, neutron beams can pass through the thick samples holder needed to keep samples in confined conditions. As such studies are rather rare, we chose to show some details of the results obtained, which also illustrate various ways of interpreting small-angle scattering data.

For a compacted dry bentonite pellet, the scattering curve recorded on line D11 at ILL displays a continuous and monotonous decrease of intensity for increasing scattering vector q (Fig. 18.7A). The background has not been subtracted and corresponds to the incoherent scattering of structural hydrogen atoms. Intensity decrease follows a power-law decay $I \propto q^{-\alpha}$, with α around 3.5 (Fig. 18.7A). In the case of rocks, such a behavior is often assigned to materials with fractal surface or to porous materials with a power-law distribution of pore sizes [82]. In the present case, the analysis of the SANS curve is based on the assumption that the system is biphasic and consists of a population of uncorrelated pores whose sizes follow a polydisperse distribution.

In that case, intensity is expressed as follows:

$$I(q) = |\Delta\rho|^2 \int_0^\infty F(q, D)V^2(D)N_{\mathrm{T}}P(D)\mathrm{d}D,$$

and for spheres

$$F(q, D) = \left(3\frac{\sin(qD/2) - (qD/2)\cos(qD/2)}{(qD/2)^3}\right)^2, \tag{18.10}$$

where D is the dimension of the particles (for spheres D is the diameter), and $F(q, D)$ is the form factor.

The volume distribution function may be defined as

$$f(D) = V(D)N_T P(D), \tag{18.11}$$

where

$V(D)$ is the particle volume,
N_T is the total number of scattering particles,
$N_T\ P(D)$ is the probability of occurrence of scatterers of size D (i.e., the number of pores between size D and $D + \mathrm{d}D$).

By intensity inversion, it is then possible to derive pore volume distribution functions $f(D)$ (Fig. 18.7B). Calculations were made using a software package, "IRENA," developed by Jan Ilavsky (Advanced Photon Source, Argonne National Laboratory, USA) and available on http://usaxs.xor.aps.anl.gov/staff/ilavsky/irena.html. The inversion was performed on the basis of a spherical pore shape. Even if this assumption does not really reflect the suspected pore shape, attempts made using elongated spheroids did not yield a better fit.

The distribution derived from the SANS curve was compared with the pore size distribution obtained on the same system by nitrogen adsorption using the Barret-Joyner-Halenda method [83]. The comparison, displayed on Fig. 18.7B, clearly shows the adequacy of both approaches, which rely on different principles. For

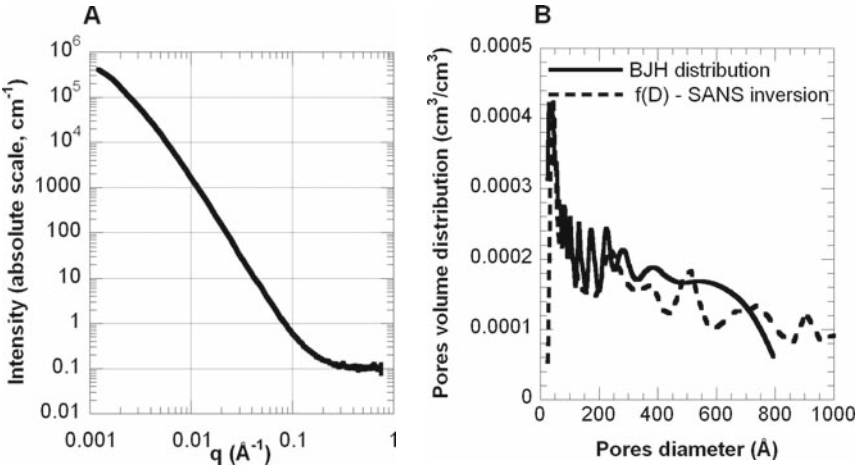

Fig. 18.7 **A**. Small-angle neutron scattering (SANS) curve recorded for a bentonite at an apparent density of 1.7 g/cm^3. **B**. Comparison of the pore volume distribution derived from SANS curves and by nitrogen adsorption using the Barret-Joyner-Halenda (BJH) method

hydrated clays, the situation is more complicated as three phases are present: (1) a hydrated clayey matrix, (2) pores filled with water, and (3) macropores that are not completely filled (with water). Interpretation based on a biphasic system then does not hold anymore. However, it is still possible to get a qualitative analysis of scattering curves and to compare various experimental conditions (Fig. 18.8).

For a relative water pressure of 0.98, the scattering curves of unconstrained samples are identical whatever the density (for reasons of clarity, curves in Fig. 18.8 are not superimposed on the same graph). In contrast, those recorded in confined conditions deviate from free swelling conditions for the lowest q values. This divergence is more marked with increasing apparent density. Thus, confinement affects mesoporosity, but a thorough characterization of this effect relies on the treatment of SANS curves for hydrated samples, which is not trivial due to the coexistence of three phases.

18.4.3 Structure of Suspensions and Gels

Suspensions of smectite dispersed in water exhibit particular rheological properties: a sol–gel transition is observed even at very low solids concentration [84]. The structure of this gel has long been an object of debate, with two mechanisms proposed to explain gel formation: (1) 3D house of cards type structure with attractive interactions between the positively charged edges and the negatively charges faces of clay layers [64] and (2) oriented network of parallel layers with repulsive electrostatic interactions between double layers [54, 85]. To unravel this issue, it is necessary to establish the correlation function between clay layers inside gels

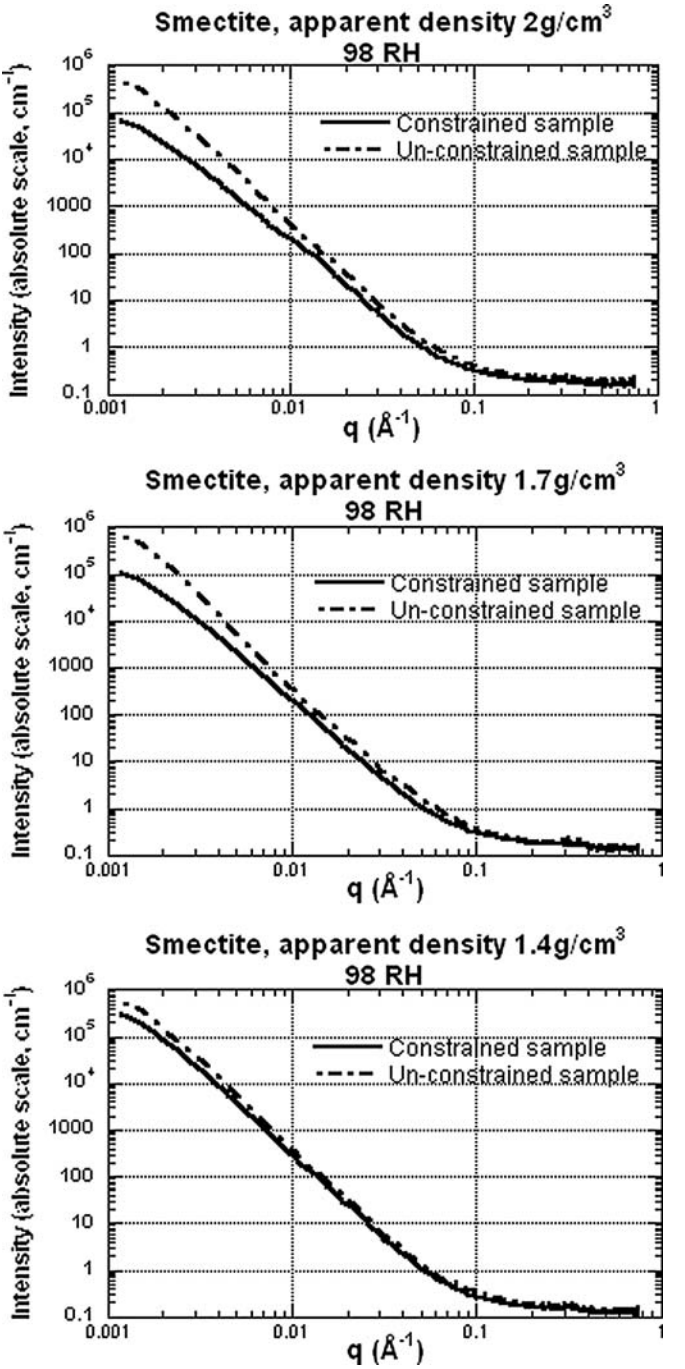

Fig. 18.8 Small-angle neutron scattering curves recorded for smectites compacted at various apparent densities, both in constrained and unconstrained swelling conditions (relative humidity of 98%)

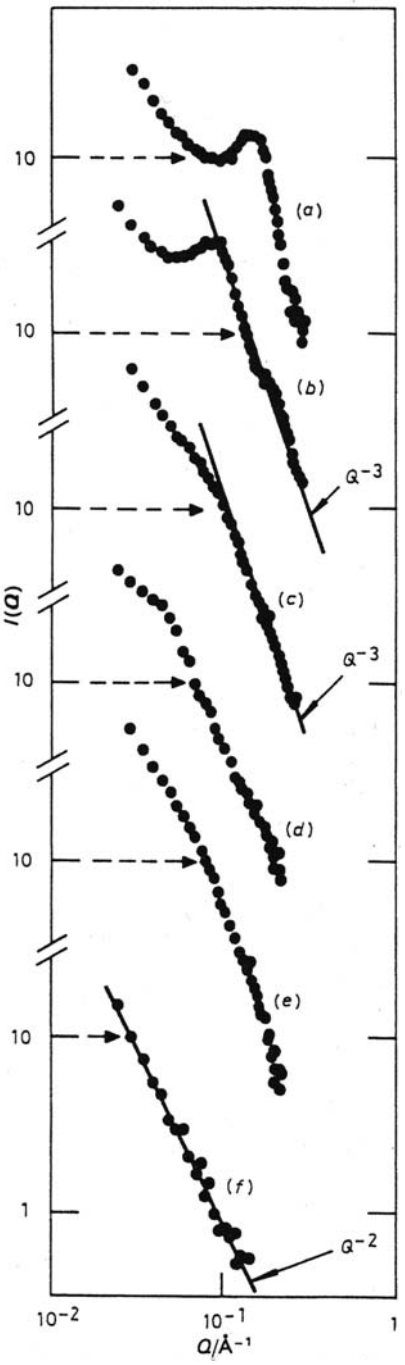

Fig. 18.9 Small-angle neutron scattering data for montmorillonite dispersed in D_2O with D_2O/montmorillonite ratios (g/g) of (a) 1.5, (b) 3.5, (c) 5.9, (d) 8.1, (e) 11.3, and (f) 22.5 (from [25]; reproduced by permission of The Royal Society of Chemistry)

and suspensions. A comprehensive SANS investigation was performed on two different smectites (montmorillonite and Laponite) as a function of solid concentration [24, 25, 27]. Examples of curves recorded on montmorillonite dispersions are shown in Fig. 18.9. For the lowest concentration, intensity follows a q^{-2} decay, which corresponds to the scattering of individual bidimensional objects without interactions. As concentration increases, a modulation appears that is represented by a well-defined diffraction peak for the highest concentrations. When plotting the evolution of this interlayer spacing as a function of water content, d spacings exhibit an inverse relationship with volume fraction, revealing a 1D swelling mechanism [25]. This demonstrates that in gels particles are equilibrated via electrostatic repulsions as suggested by Norrish [54]. This dependence of d spacing on clay concentration was confirmed with other smectites (montmorillonite [86], nontronite [87], and laponite [34]).

In cases of suspensions, it is worth mentioning that SANS patterns can be recorded under flow using various rheological devices. For example, this was implemented in the case of swelling clay gels in a Couette-type cell [27]. Other work aiming at understanding clay-based nanocomposites have also used such devices to follow the structural evolution of clay-polymer mixtures [29–32].

18.5 Conclusion

Because of their versatility and specific features, neutron-based techniques are particularly relevant for studying various aspects of clay swelling, a multiscale process extending over several orders of magnitude in space. At the atomic level, the sensitivity of neutrons to hydrogen isotopes allows a detailed refinement of both structure and amount of interlayer water, which should help in addressing the force fields used for molecular simulations of the clay–water interface. The same type of comparison between simulation and experiments can then be applied to the dynamics of interlayer water, which can be studied at various time scales and for various orientations, taking advantage of the different experimental setups (TOF, BS, NSE, triple-axis spectrometer) available in neutron facilities (Chapter 3).

From an experimental point of view, for hydration measurements for water chemical activity between 0 and 0.98, a very accurate control of the water partial pressure is needed, with also a precise analysis of the hydration properties of the sample being investigated. Indeed, it was demonstrated that the hydration behavior is strongly dependent on the clay crystal-chemistry, which should be established first. In addition, the swelling properties of each sample should be established by combining other independent techniques such as gravimetry measurements or spectroscopy experiments.

At the submicronic scale, the ability of neutrons to probe the structure and texture of large and dense samples under various experimental conditions (pressure, temperature, P_{H2O}, shear, etc.) clearly presents a key advantage for assessing the behavior of clay samples in natural or industrial situations. Due to the neutron penetration

length, complex sample conditions can be adapted to carry out experiments at non-ambient temperatures and/or pressures. These conditions can be achieved either by adapting the available equipment at neutron facilities or by developing homemade devices. This versatility in sample environment represents a clear advantage of neutrons over X-rays.

Acknowledgments We thank Jean-Louis Robert (ISTO, Orléans, France) for providing us with synthetic saponite. Experimental support by Karine Devineau, Eric Ferrage, Solange Maddi, Manuel Pelletier, Angelina Razafitianamaharavo, Cedric Carteret, Emmanuel Rinnert, and Bernard Humbert during campaigns at ILL is warmly acknowledged. We thank Giovana Fragneto for technical assistance on D16. Institut Laue-Langevin is acknowledged for beam-time allocation. A part of this work was funded by ANDRA (French national agency for radioactive waste management).

References

1. Harvey C.C., Lagaly G., *Handbook of Clay Science*, edited by F. Bergaya, B. K. G. Theng, G. Lagaly (Elsevier, Oxford, 2006) pp. 501–540
2. Dove M. T., Eur. J. Mineral., **14**, 203 (2002)
3. Cebula, D. J., Thomas, R. K., Middleton, S., Ottewill, R. H., White, J. W., Clays Clay Miner., **27**, 39 (1979)
4. Hawkins, R. K., Egelstaff, P. A., Clays Clay Miner., **28**, 19 (1980)
5. Joswig W., Fuess H., Mason S.A., Clays Clay Miner., **37**, 511 (1989)
6. Skipper N. T., Soper A. K., McConnell J. D. C., Refson K., Chem. Phys. Lett., **166**, 141 (1990)
7. Skipper N. T., Soper A. K., McConnell J. D. C., J. Chem. Phys., **94**, 5751 (1991)
8. Skipper N. T., Soper A. K., Smalley M. V., J. Phys. Chem., **98**, 942 (1994)
9. Skipper N. T., Smalley M. V., Williams G. D., Soper A., Thompson C. H., J. Phys. Chem., **99**, 14201 (1995)
10. Akiba E., Hayakawa H., Hayashi S., Miyawaki R., Tomura S., Shibasaki Y., Izumi F., Asano H., Kamiyama T., Clays Clay Miner., **45**, 781 (1997)
11. Powell, D. H., Tongkhao, K., Kennedy, S. J., Slade, P. G., Clays Clay Miner., **45**, 290 (1997)
12. Powell, D. H., Tongkhao, K., Kennedy, S. J., Slade, P. G., Physica B, **243**, 387 (1998)
13. Williams G. D., Soper A. K., Skipper N. T., Smalley, M. V., J. Phys. Chem. B, **102**, 8945 (1998)
14. Sposito G, Park S.-H., Sutton R., Clays Clay Miner., **47**, 192 (1999)
15. Skipper N. T., Williams, G. D., de Siqueira A. V. C., Lobban C., Soper A. K., Clay Miner., **35**, 283 (2000)
16. Pitteloud C., Powell D. H., Fischer H. E., Phys. Chem. Chem. Phys., **3**, 5576 (2001)
17. Swenson J., Smalley M. V., Hatharasinghe, H. L. M., Fragneto G., Langmuir, **17**, 3813 (2001)
18. Beyer J, Graf von Reichenbach H., Clay Miner., **37**, 157 (2002)
19. Wasse, J. C., Stebbings, S. L., Masmanidis, S., Hayama, S., Skipper, N. T., J. Molec. Liq., **96**, 341 (2002)
20. Perdigon-Aller A. C., Aston M., Clarke S. M., J. Colloid Interface Sci., **290**, 155 (2005)
21. Rinnert E., Carteret C., Humbert B., Fragneto-Cusani G., Ramsay J. D. F., Delville A., Robert J. L., Bihannic I., Pelletier M., Michot J. L., J. Phys. Chem. B, **109**, 23745 (2005)
22. Devineau K., Bihannic I., Michot L. J., Villiéras F., Masrouri F., Cuisinier O., Fragneto G., Michau N., Appl. Clay Sci., **31**, 76 (2006)
23. Malikova N., Cadène A., Dubois E., Marry V., Durand-Vidal S., Turq P., Breu J., Longeville S., Zanotti J.-M., J. Phys. Chem. C, **111**, 17603 (2007)
24. Avery, R. G., Ramsay, J. D. F., J. Colloid Interf. Sci., **109**, 448 (1986)

25. Ramsay, J. D. F., Swanton, S. W., Bunce, J. J. Chem. Soc. Faraday Trans., **86**, 3919 (1990).
26. Allen A. J., J. Appl. Cryst., **24**, 624 (1991)
27. Ramsay, J. D. F., Lindner, P., J. Chem. Soc. Faraday Trans., **89**, 4207 (1993)
28. Hanley H. J. M., Straty G. C., Tsvetkov F., Langmuir, **10**, 3362 (1994)
29. Grillo I., Levitz P., Zemb T., Eur. Phys. J. B, **10**, 29 (1999)
30. Schmidt G., Nakatani A. I., Butler P. D., Karim A., Han C. C., Macromolecules, **35**, 7219 (2000)
31. Schmidt G., Nakatani A. I., Butler P. D., Karim A., Han C. C., Macromolecules, **33**, 4725 (2002)
32. Nettesheim F., Grillo I., Lindner P., Richtering, W., Langmuir, **20**, 3947 (2004)
33. Itakura T., Bertram W. K., Knott R. B., Appl. Clay Sci., **29**, 1 (2005)
34. Martin C., Pignon F., Magnin A., Meireles M., Lelièvre V., Lindner P., Cabane B., Langmuir, **22**, 4065 (2006)
35. Olejnik S., Stirling G. C., White J. W., Spec. Disc. Faraday Soc., **1**, 194 (1970)
36. Dianoux A. J., Volino F., Hervet H., Mol. Phys., **30**, 1181 (1975)
37. Cebula, D. J., Thomas, R. K., White, J. W., Clays Clay Min., **29**, 241 (1981)
38. Tuck J. J., Hall P., Hayes M. H. B., Ross D. K., Poinsignon C., J. Chem. Soc. Faraday Trans., **80**, 309 (1984)
39. Tuck J. J., Hall P., Hayes M. H. B., Ross D. K., Hayter J. K., J. Chem. Soc. Faraday Trans., **81**, 833 (1985)
40. Poinsignon C., Estrade-Schwarzckopf J., Conard J., Dianoux A. J., *Proc. Intl. Clay Conference*, edited by L. G. Schultz, H. Van Olphen, F. A. Mumpton (The Clay Minerals Society, Bloomington, Indiana, 1987), p. 284
41. Poinsignon C., Solid State Ionics, **97**, 399 (1997)
42. Swenson J., Bergman R., Howells W. S., J. Chem. Phys., **113**, 2873 (2000)
43. Swenson J., Bergman R., Longeville S.., Howells W. S., Physica B, **301**, 28 (1991)
44. Swenson J., Bergman R., Longeville, S., J. Chem. Phys., **115**, 11299 (2001)
45. Mamontov, E., J. Chem. Phys., **121**, 9193 (2004)
46. Malikova N., Cadene A., Marry V., Dubois E., Turq P., Zanotti J.-M., Longeville S. J., Chem. Phys., **317**, 226 (2005)
47. Chakrabarty D., Gautam S., Mitra S., Gil A., Vicente M. A., Mukhopadhyay R., Chem. Phys. Lett., **426**, 296 (2006)
48. Malikova N., Cadene A., Marry V., Dubois E., Turq P., J. Phys. Chem. B, **110**, 3206 (2006)
49. Skipper N. T., Lock P. A., Tililoye J. O., Swenson J., Mirza, Z. A., Howells, W. S., Fernandez-Alonso, F., Chem. Geol., 230, **182** (2006)
50. Michot L. J., Delville A., Humbert B., Plazanet M., Levitz P., J. Phys Chem. C, **111**, 9818 (2007)
51. Newman A. C. D., *Chemistry of Clays and Clay Minerals* (Mineralogical Society, London, 1987)
52. IUPAC Manual of symbols and terminology for physico-chemical quantities and units, Appendix 2, Definitions, Terminology, and Symbols in Colloid and Surface Chemistry. Part 1. Pure Appl Chem **31**, 578 (1972)
53. Bihannic I., Tchoubar D., Lyonnard S., Besson G., Thomas F. J., Colloid Interface Sci., **240**, 211 (2001)
54. Norrish K., Quirk J. P., Nature, **173**, 225–256 (1954)
55. Mooney R. W., Keenan A. G., Wood, L. A., J. Amer. Chem. Soc., **74**, 1371 (1952)
56. Norrish K., Raussell-Colom, J. A., Clays Clays Miner., **10**, 123 (1963)
57. Sposito G., Prost R., Chem. Rev., **82**, 553 (1982)
58. Glaeser R., Méring J., C.R. Acad. Sci. Paris, **T. 267 Série D**, 463 (1968)
59. Suquet H., Pezerat H., Clays Clay Miner., **35**, 353 (1987)
60. Michot L. J., Bihannic I., Pelletier M., Rinnert E., Robert J.-L., Am. Miner., **90**, 166 (2005)
61. Ferrage E., Lanson B., Sakharov B. A., Drits V. A., Am. Miner., **90**, 1358 (2005)
62. Bérend I., Cases J. M., François M., Uriot J. P., Michot L. J., Masion A., Thomas F., Clays Clay Miner., **43**, 324 (1995)

63. Cases J. M., Berend I., François M., Uriot J. P., Michot L. J., Thomas F., Clays Clay Miner., **45**, 8 (1997)
64. Van Olphen, H., *An Introduction to Clay Colloid Chemistry*, 2nd ed. (John Wiley & Sons, New York, 1977)
65. Güven, N., *Clay-water Interface and Its Rheological Implications*, edited by N. Güven, R. M. Pollastro (CMS Workshop Lectures, Clay Minerals Society, Boulder, CO, USA, 1992) p. 2
66. Marry V., Turq P., J. Phys. Chem. B, **107**, 1832 (2003)
67. Chang F.-R. C., Skipper N. T., Sposito G., Langmuir, **11**, 2734 (1995)
68. Nagelschmidt G., Zeit. Kristall. **93**, 481 (1936)
69. Bradley W. F., Grim R. E., Clark G. F., Zeit. Kristall. **97**, 260 (1940)
70. De la Calle C., Suquet H., Dubernat J., Pezerat, H., Clay Miner., **13**, 275 (1978)
71. Push R., *Handbook of Clay Science*, edited by F. Bergaya, B. K. G. Theng, G. Lagaly (Elsevier, Amsterdam, London, 2006) pp. 703–716
72. Drits V. A., Tchoubar C., *X-Ray Diffraction by Disordered Lamellar Structure. Theory and Applications to Microdivided Silicates and Carbons* (Springer-Verlag, Berlin, 1990)
73. Mering J., Acta Cryst., **2**, 371 (1949)
74. Bée, M.. *Quasi-Elastic Neutron Scattering* (Adam Hilger, Philadelphia, PA, 1988)
75. Bée M., Chem. Phys., **292**, 121 (2003)
76. Egelstaff P. A., *An Introduction to the Liquid State* (Clarendon, Oxford, UK, 1992)
77. Glatter O., Kratky O., *Small Angle X-ray Scattering* (Academic Press Inc., London, 1982)
78. Brumberger H., *Modern Aspects of Small-angle Scattering* (NATO ASI Series C, Vol. 451, Kluwer Academic Publishers, Dordrecht, 1995)
79. Lindner P., Zemb T., *Neutron, X-rays and Light: Scattering Methods Applied to Soft Condensed Matter* (North Holland, Amsterdam, 2002)
80. Madsen F. T., Clay Miner., **33**, 109–129 (1998)
81. Komine H., Ogata, N., Can. Geotech. J. **31**, 478 (1994)
82. Radlinski A. P., *Neutrons Scattering in Earth Sciences*, edited by J. J. Rosso (The Mineralogical Society of America, 2006)
83. Barett E. P., Joyner L. G., Halenda P. H., J. Am. Chem. Soc., **73**, 373 (1951)
84. Mourchid A., Lecolier E., Van Damme H., Levitz, P., Langmuir, **14**, 4718 (1998)
85. Callaghan I. C., Ottewill, R., Chem. Soc., **57**, 110 (1974)
86. Michot L. J., Bihannic I., Maddi S., Funari S., Baravian C., Levitz P., Davidson P., Proc. Natl. Acad. Sci., **103**, 16101 (2006)
87. Michot L. J., Bihannic I., Maddi S., Baravian C., Levitz P., Davidson P., Langmuir, **24**; 3127 (2008).